J Mater Sci (2009) 44:1580–1587
DOI 10.1007/s10853-008-3242-5

Machinability, deformation, and cracks behavior of pressureless-sintered Al_2O_3/h-BN composites: role of weak boundary phases

Zhongqi Shi · Jiping Wang · Guanjun Qiao · Jianfeng Yang · Zhihao Jin

Received: 7 October 2008 / Accepted: 31 December 2008 / Published online: 27 January 2009

Abstract Al_2O_3/h–BN machinable composites were cost-effectively fabricated by pressureless sintering method. The machinability, deformation, and cracks behavior of the composites were investigated by drilling, Hertzian indentation, and Vickers indentation test, respectively. Through the observation of the microstructures in different scales by SEM, we analyzed the role of the weak boundary phases (WBP), including h-BN and pores, on the machining mechanism of the composites. The results showed that almost all of the WBP dispersed at the Al_2O_3 grain boundaries, which strongly elevate the machinability and deformability of the composites. During the drilling or Hertzian indentation test, a large number of microcracks formed firstly along the WBP; then these microcracks connected with each other causing a removal or macro-deformation of the composites. The Vickers indentation test result indicated that the weak interfaces and grain boundaries of WBP lead to a low microcrack toughness, whereas in macro-scale the crack toughness was improved because of the crack bridging and deflection of WBP.

Introduction

Machinable ceramics are a new type of advanced material, and they can be easily machined by conventional metal tools into complicated shapes for the applications with required precision. Recently, various machinable ceramics have been developed through introducing different weak boundary phases (WBP) in matrices. The WBP include mica [1], h-BN [2–5], graphite [6], YAG [7], rare-earth phosphates [8], pores [9, 10], and Ti_3SiC_2 analogous compounds [11]. Usually, these WBP possess weak layered crystal structure or can introduce weak interfaces into the matrices.

Among the developed machinable ceramics, h-BN contained ceramics showed good machinability, together with excellent corrosion resistance to molten metals and high thermal shock resistance. However, the composites are usually prepared by hot-pressing, which restricts its application because the processing costs highly and is unable to prepare complex shape components. Recently, we prepared Al_2O_3/h-BN machinable composites by the economical pressureless sintering method [12]. The effects of WBP on the microstructure and mechanical properties of the composites were also investigated. When h-BN added, the composites are porous because of the poor sinterability of h-BN which has strong covalent nature and plate-like structure. As a result, two kinds of WBP exist in the Al_2O_3/h-BN composites, including h-BN and pores, which could strongly control the mechanical properties and machinability. We found that the composites containing 10 vol.% h-BN (relative porosity 8.8%), exhibited both high mechanical properties and good machinability. However, what is the role of the WBP influence the machinability of the composites is not clear.

In order to well understand the machining mechanism and materials removal process, it is particularly interested to study the deformation mechanisms and cracks expansion behavior of the machinable ceramics. The deformation behaviors of some machinable composites, such as SiC/YAG [13], Si_3N_4/h-BN [14], and micaceous glass–ceramic [15], have been investigated formerly. It revealed that the quasi-plastic deformation behavior is the main reason for

Z. Shi (✉) · J. Wang · G. Qiao · J. Yang · Z. Jin
State Key Laboratory for Mechanical Behavior of Materials, School of Materials Science and Engineering, Xi'an Jiaotong University, Xi'an 710049, People's Republic of China
e-mail: szqxjtu@gmail.com

good machinability. Furthermore, the researches on the cracks extension behavior of the machinable ceramics revealed that the mechanism of materials removal has strong relationship with the slow rising toughness curves behavior due to the weak-interface cracks bridging [16, 17]. However, according to the best of our knowledge, the effects of two kinds of WBP on the machinability of the ceramic composites have not been reported yet.

Therefore, in this article, the role of WBP, including h-BN and pores, on the machinability and deformation of the Al_2O_3/h-BN composites are studied. Additionally, the cracks (microcracks and macrocracks) behaviors of the composites are also discussed.

Experimental procedure

The pressureless sintering process for fabrication of Al_2O_3/h-BN composites was described in our previous literature [12]. The starting powders were α-Al_2O_3 (2 μm), h-BN (4 μm), and 3 wt% of MgO as sintering aid. The powders were mixed by ball-milling in ethanol, and then drying and sieving. The powder mixture was uniaxially pressed into rectangular green compacts and then cold isostatically pressed at 200 MPa. The green compacts were pressureless sintered at 1750 °C for 2 h in N_2 atmosphere. The sintered compacts were treated by cutting, grinding, and polishing for the following measurements. Table 1 shows the typical properties of the composites [12]. For simplicity, the composites contained 10, 15, and 20 vol.% h-BN were denoted as AB10, AB15, and AB20, respectively.

The machinability was evaluated using cemented carbide drills with the diameter of 2.5 mm. In this test, the specimens were fastened to a plate. They were drilled with a rotational speed of 500 rpm under different axial loads ranged from 1 to 12 N. In order to reduce errors in measurement, new drills were used for each test. The drilling velocity (V) was calculated according to the following equation:

$$V = \frac{H}{t}, \tag{1}$$

where H is the drilling depth and t is the drilling time. For accuracy, each test was done thrice, and the drilling velocity was the average value.

Hertzian indentation tests were performed at a constant crosshead speed of 0.5 mm min^{-1} over a load of 100 N, using tungsten carbide spheres of radius $r = 1.67$ mm. In order to investigate the subsurface contact damage, sectional views of the damage patterns were obtained using bonded interface specimens [13]. The samples were prepared by bonding together two polished half-bars with a thin layer of adhesive, and then polishing the top surfaces. Hertzian indentations were performed at the top surfaces symmetrically along the surface trace of the bonded interface. Finally, the adhesive was dissolved and cleaned using acetone.

In order to investigate the influence of WBP on the macrocracks expansion, Vickers indentation method was used with a load of 49 N on the polished surfaces of the samples.

The microstructure characterization of the specimens on fractured sections, drilled surfaces, drilled debris, contact-damaged zones, and macrocracks expansion paths were performed using a JSM 6460 (JEOL) SEM.

Results and discussion

Microstructure of the WBP in the composites

Figure 1 shows the SEM micrographs of fracture surfaces of the Al_2O_3/h-BN composites. It can be noticed that both of the composites AB10 and AB20 are porous, and the residual pores are near the h-BN platelets. Nearly all of the WBP, including h-BN and pores, exist at the grain boundaries of the Al_2O_3 matrix (Fig. 1b, d). These intergranular WBP weaken the strength of the grain boundaries, and act as fracture sources in the composites. Furthermore, it has been reported that machinability is caused by the weak interface between matrix grains and second phases at grain boundaries [14]. Therefore, the mechanical properties and machinability of the Al_2O_3/h-BN composites can be intensively influenced by the WBP [12].

Machinability and machining surface analysis

Figure 2 shows the test results of drilling velocity under different axial drilling loads for the Al_2O_3/h-BN

Table 1 Typical properties of the Al_2O_3/h-BN composites [12]

Sample	Relative density (%)	Porosity (%)	h-BN content (vol.%)	WBP content (vol.%)	σ_f (MPa)	K_{IC} (MPa $m^{1/2}$)	H_V (GPa)	E (GPa)
AB10	91.2	8.8	10	18.8	310	3.4	8.1	271
AB15	88.6	11.4	15	26.4	209	2.6	6.8	233
AB20	83.3	16.7	20	36.7	141	1.4	3.9	193

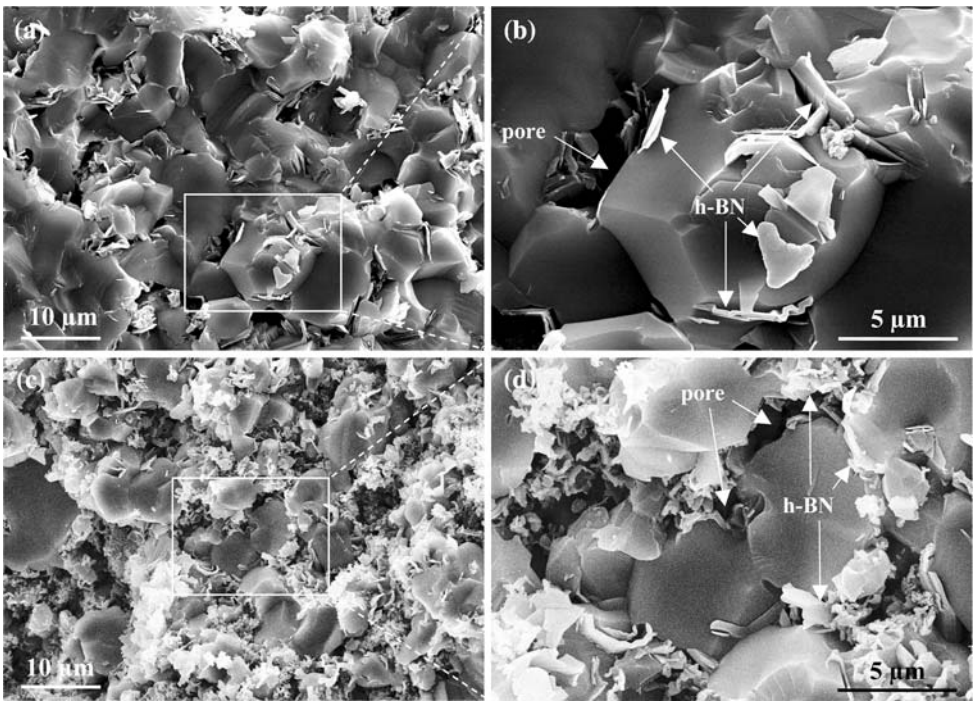

Fig. 1 **a**, **c** SEM micrographs of fracture surfaces in the sample AB10 and AB20, respectively; **b**, **d** magnified micrographs of the rectangular areas in (**a**) and (**c**), respectively

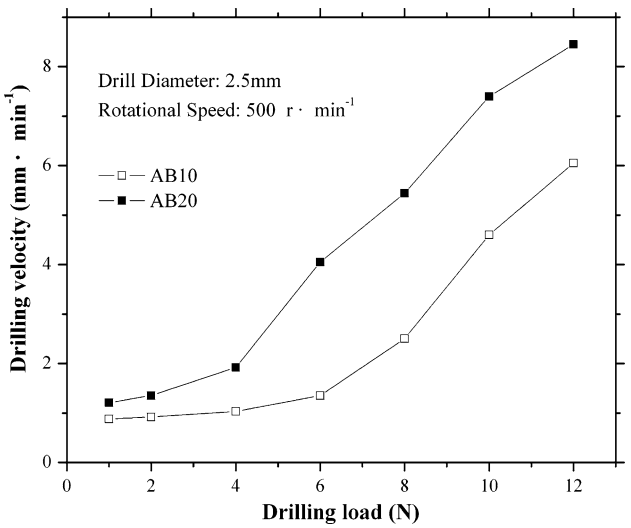

Fig. 2 Measurements of drilling velocity as a function of drilling load for AB10 and AB20

composites. It can be seen that the drilling velocities for AB10 and AB20 increase with increasing drilling load. The drilling velocity for AB20 is higher than that of AB10. It is also found that there exist the critical loads for the drilling tests, suggesting that the composites could be machined easily with the drilling load higher than the critical value. The critical drilling loads are about 4 and 8 N for AB20 and AB10, respectively.

Figure 3 shows the SEM micrographs of the drilled surface of the composites. It can be noticed that both of the drilled surfaces of AB10 and AB20 are smooth and without obvious cracks. The surfaces are partly covered with a layer of smeared debris. The drilled debris of the composites are revealed in Fig. 4. It can be seen that the particle surfaces of the debris are smooth, and their particle sizes are similar with the Al_2O_3 grains in matrices (see Fig. 1). Therefore, one can conclude that the intergranular fracture of Al_2O_3 grains is predominant during the machining process, and these WBP evaluate the removal of these hard Al_2O_3 grains, which endows the composites with excellent machinability. Actually, it is difficult to distinguish which WBP is more important for promoting the machinability because of their cooperatively effect during the machining process. However, we can undoubtedly believe the promoting effect of h-BN or pores on the machinability of the composites, which has been approved by many literatures reported before [2–5, 9, 10].

Deformation behavior after Hertzian contact test

In order to investigate the machining mechanism of the composites, Hertzian contact tests were performed as other literatures reported [13, 14, 18]. The stress condition in the tests is similar to the machining process. The composite contained 20 vol.% h-BN was selected as the subject in order to investigate in the tests since it possesses more WBP content (36.7 vol.%) besides good machinability. Figure 5 shows the SEM micrographs of Hertzian contact damage in the composite. The damage in

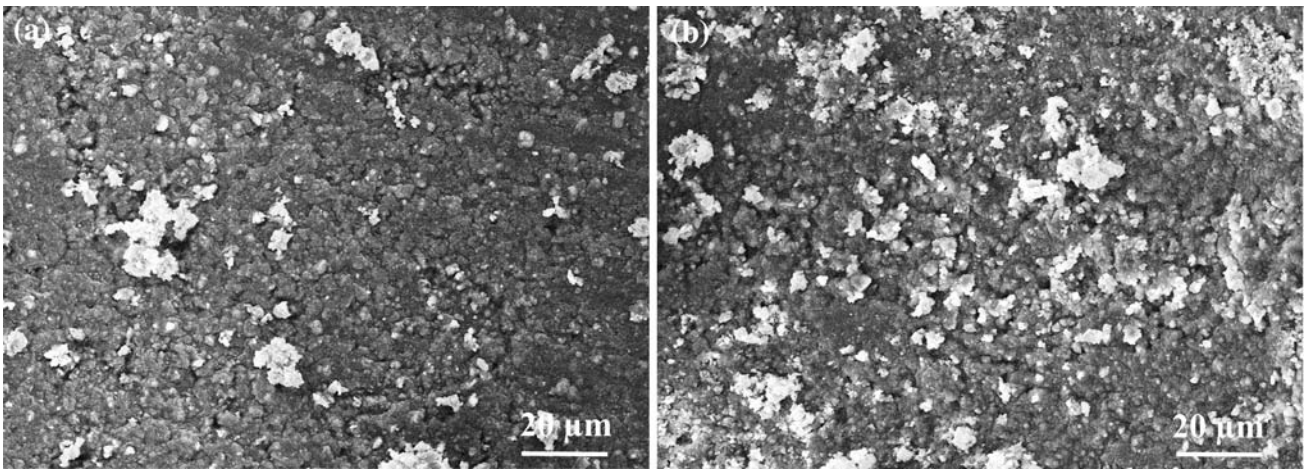

Fig. 3 SEM micrographs of the drilled surface of AB10 and AB20

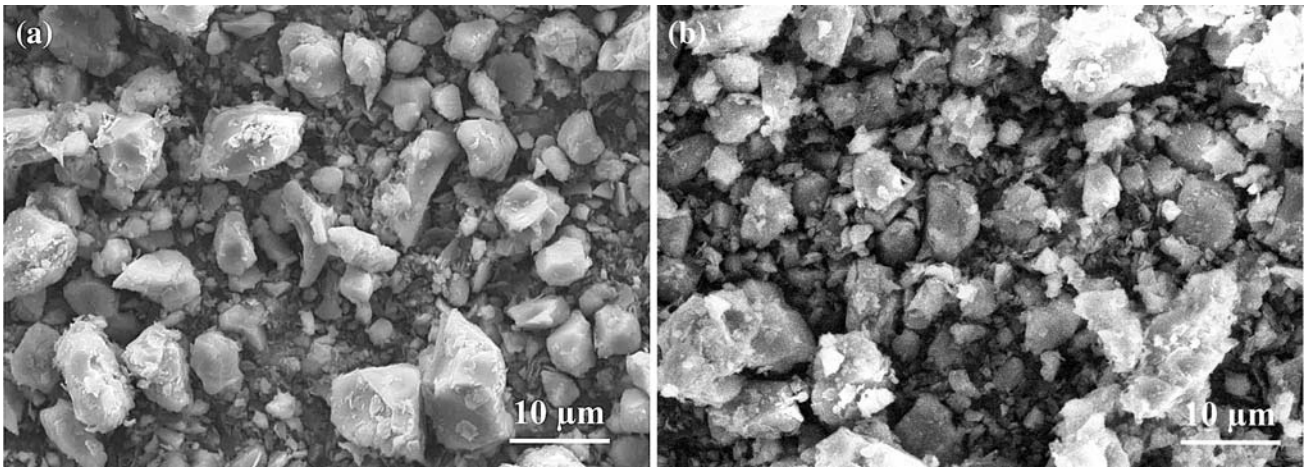

Fig. 4 SEM micrographs of the drilled debris of AB10 and AB20

the subsurface deformation zone appears to be quasi-plastic deformation, reminiscent of the plastic deformation zone in ductile metals (Fig. 5a). Moreover, there is no obvious macrocracks penetrating downward into the inner part of the composite. It is evidently different from the classical Hertzian cone crack observed in the monolithic Al_2O_3 [19]. Figure 5b shows the high-magnified micrograph of Fig. 5a. One can notice that there are three different zones beneath the contact surface: large-deformation zone (Fig. 5c), microcracks zone (Fig. 5d), and matrix zone. These zones have clear boundaries, and the boundary shapes are almost identical to the trajectory of principal shear stress. This result indicates that the shear stress is the key reason for the contact damage, which has been approved by Cai et al. [15]. Comparing the micrographs between the large-deformation zone and the microcracks zone (Fig. 5c, d), it can be noticed that in both zones, a large number of microcracks formed along the WBP, with some linkages and coalescence of WBP. Under the subsurface Hertzian stress field, the WBP provide favored paths for the extension of microcracks along the weak interfaces. Nearly all of the pores vanished in the large-deformation zone. However, the pores still exist in the microcracks zone. This can be attributed to the different stress intensity between the two zones. In large-deformation zone, the stress intensity is higher than in microcracks zone, which makes the deformation of the pores more seriously. Furthermore, the deformation of the h-BN grains can also be observed beneath the contact surface, as shown in Fig. 5e. It is apparent that delamination and kinking are two basic deformation and damage modes for h-BN grain beneath the contact surface. The microcracks are formed along the h-BN basal plane, as indicated by arrows in Fig. 5e.

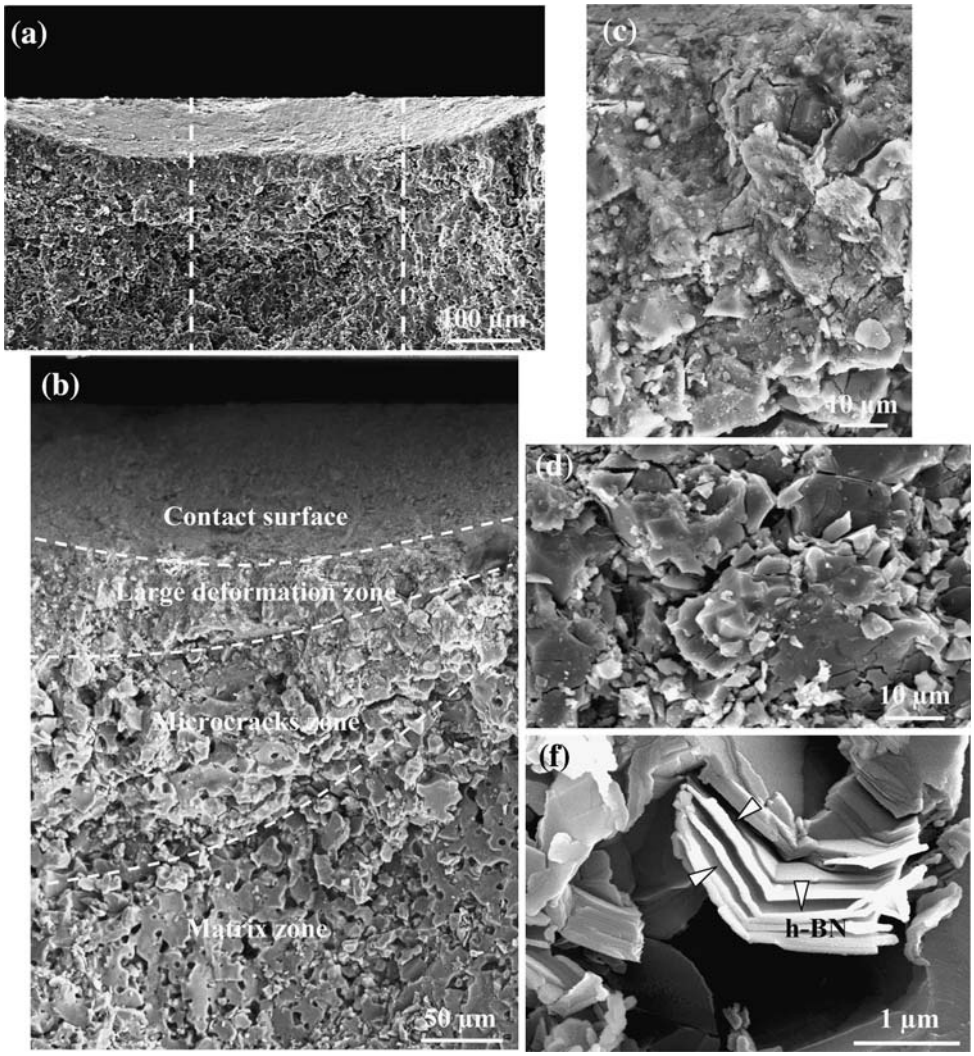

Fig. 5 SEM micrographs of Hertzian contact damage in AB20: **a** quasi-plastic deformation zone; **b** high-magnified area of (**a**); **c**, **d** represent large-deformation zone and microcracks zone in (**b**); **e** deformation and damage of h-BN beneath the contact surface

From the observation and discussion above, we can conclude that the quasi-plastic deformation process in Al_2O_3/h-BN composites includes two steps. First, a large number of microcracks were formed along the WBP. Then the microcracks linked each other with the deformation of WBP. Thus, the WBP promote the formation of microcracks in the Al_2O_3/h-BN composites, and enhance the capacity for energy absorption from contacts and impacts, preventing the catastrophic failure. As a result, the cracks are restricted in a small zone, where the particles can be flaked off easily during the machining process.

Model of microcracks linkages

A shear-fault/wing-crack model [20] can well explain the effect of WBP on the microcracks linkages in the Al_2O_3/h-BN composites during the machining and Hertzian contact tests. Figure 6a shows a schematic representation of the microstructure of the composites, according to the microstructure characteristic shown in Fig. 1b and d. When a Hertzian contact load, P, forces on the surface of the composites, a large number of microcracks formed along the WBP in the damage zone. Then, the composites would be supported only by the bonding strength of Al_2O_3 matrix grains boundaries, and they will be the slip planes in the deformation process. As shown in Fig. 6b, τ_θ and σ_θ are local shear stress and normal stress on the slip plane and can be expressed as below:

$$\tau_\theta = \sigma \cdot \cos\theta \cdot \sin\theta, \tag{2}$$

$$\sigma_\theta = \sigma \cdot \sin^2\theta, \tag{3}$$

where σ is the applied compressive stress and θ is the angle between the loading direction and the slip plane. Thus, the critical stress on the slip plane can be described using a Mohr–Coulomb criterion [21]:

$$\tau_C \leq \tau_\theta - \mu \cdot \sigma_\theta, \tag{4}$$

where τ_C is the net shear stress and μ is the coefficient of sliding friction. Substituting τ_θ and σ_θ into Eq. 4, the

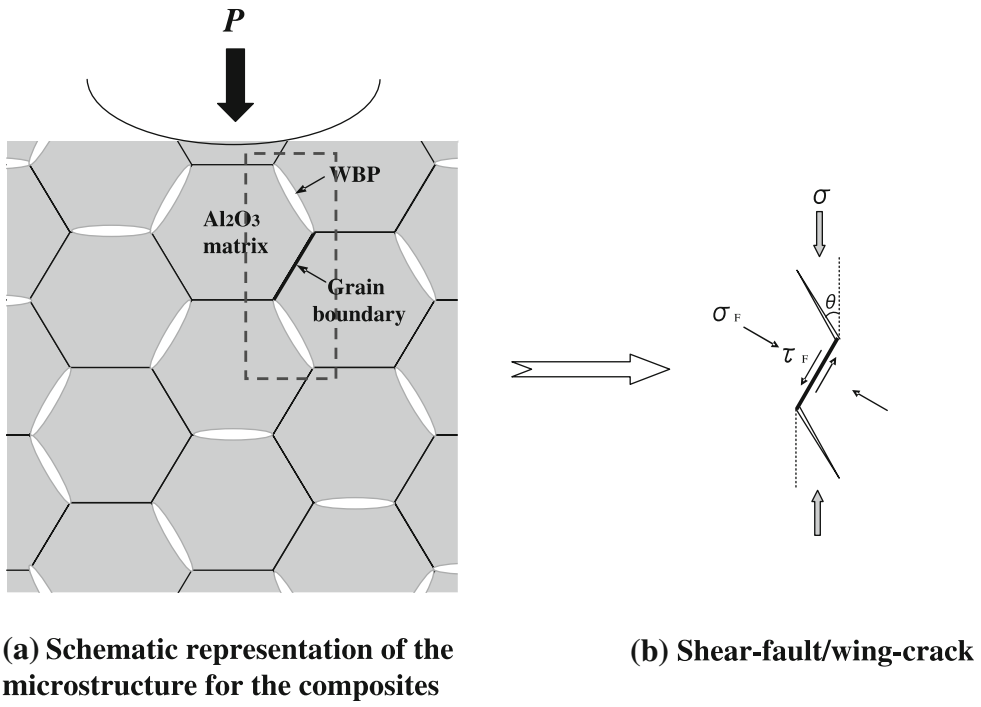

Fig. 6 Model of microcracks linkages during Hertzian contact process: **a** schematic representation of the microstructure for the composites with a load of P; **b** shear faults with individual microcrack linkage

critical fracture condition for the slip plane can be expressed as

$$\sigma_C \geq \frac{\tau_C}{\sin\theta \cdot (\cos\theta - \mu \cdot \sin\theta)}, \quad (5)$$

where σ_C is the applied compressive stress at shear fracture. So if the applied compressive stress σ is higher than the minimum fracture stress σ_C, the slip plane will fracture and the microcracks induced by WBP will be linked. Hence, the test results of drilling velocity for the composites shown in Fig. 2 can be explained as follows. In the case of the drilling load is lower than the critical value, the composite cannot be machined easily because σ_C in the drilling zone is not higher than the bonding strength of Al_2O_3 grain boundary. However, with the drilling load increases, σ_C conquers the resistance of the grain boundaries and deforms the composites, leading to the individual particles flaked off. With further increasing the drilling load, more and more microcracks could be linked to form a net-like microcracks zone, and hence increases the drilling velocity remarkably. In addition, considering the WBP content of AB20 is higher than that of AB10, the induced microcracks have a higher probability to connect (lower τ_C and σ_C vaules), which makes AB20 possesses better machinability (lower P value).

Therefore, the promoting effect of WBP on the microcracks linkages can be comprehended. WBP tailor a large amount of weak-interface structures into the machinable composites, and these structures create the faults, and also provide favored paths for ensuing extensile microcracks at the fault edges (Al_2O_3 grain boundaries) by shear stress, within the machining or deformation zone.

Macrocracks expansion after Vickers indentation test

As discussed in the above section, the microcracks in the composites can be linked easily during the machining or deformation process. But, why there is no obvious macrocracks penetrating downward into the composite during the process? Lawn et al. [13] reported that by introducing weak interfaces into the composites, any downward propagating macrocracks can be deflected along the grains or interface boundaries away from the tensile stress trajectories. So penetration downward into the composites was suppressed. In this study, both h-BN and pores as WBP also have the suppress effect to the macrocracks. Figure 7 shows the SEM morphologies of macrocrack expansion path in AB15 obtained by Vickers indentation method. As indicated by arrows in Fig. 7a and b, the crack of the composite propagates preferentially along the WBP or their interfaces, resulting crack bridging, deflection, or a tortuous crack path. As a result, the stress concentration around the crack tip is relieved and the deflection would consume much energy in this process, which prevents catastrophic failure in machining process.

According to the discussion above, WBP promote the formation of a large number of distributed microcracks beneath the machining or deformation zone, and the microcracks can be linked easily (low microcrack toughness). Meanwhile, WBP prevent the macrocracks

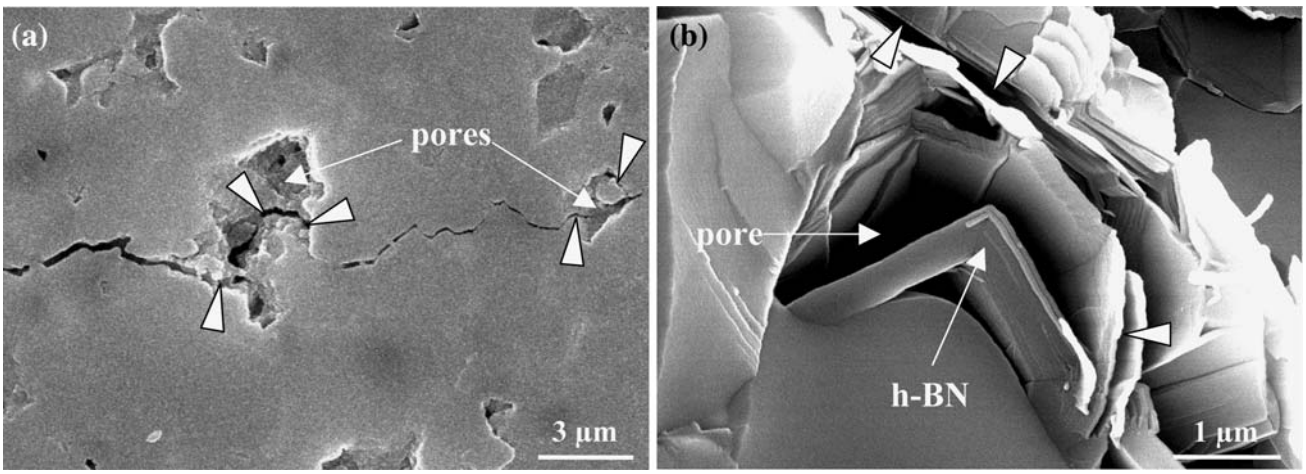

Fig. 7 SEM morphologies of macrocrack expansion path by Vickers indentation in AB15

propagating deeply into the composites during the machining or deformation process due to the high crack extension resistance (high macrocrack toughness). In other words, the Al_2O_3/h-BN composites may exhibit a slowly raising Crack-Growth-Resistance (R-curve) behavior attributed to the WBP. This slowly raising R-curve behavior is very important for the machinability of the composites [22–24]. However, in this study, it is difficult to obtain typical slow raising R-curve, because of the influence of the residual pores.

In general, WBP are considered to be the key factor to maintain good machinability and high machining accuracy since they endow the machinable composites with not only good quasi-plastic deformation ability, but also a slowly raising R-curve behavior.

Conclusion

The effects of WBP, including h-BN and residual pores, on the machinability, deformation, and cracks behavior of pressureless-sintered Al_2O_3/h-BN composites were investigated. Our conclusions can be summarized as follows:

1. Nearly all of the WBP dispersed at the grain boundaries in the composites. These intergranular WBP elevated the machinability and deformability due to their easy deformation and cleavage characteristics.
2. Quasi-plastic deformation process includes two steps. First, formation of a large number of microcracks along WBP; second, the microcracks linkages going with large deformation of WBP.
3. WBP enhance the machinability of the composites resulting from the low microcracks toughness due to their weak interfaces and grain boundaries, and improving macrocracks toughness as a result of crack bridging and deflection.

Acknowledgement This study was funded by National Natural Science Foundation of China (No. 50772086).

References

1. Grossman DG (1972) J Am Ceram Soc 55:446. doi:10.1111/j.1151-2916.1972.tb11337.x
2. Kusunose T, Sekino T, Choa YH, Niihara K (2002) J Am Ceram Soc 85:2678. doi:10.1111/j.1151-2916.2002.tb00514.x
3. Li YL, Qiao GJ, Jin ZH (2002) Mater Res Bull 37:1401. doi:10.1016/S0025-5408(02)00786-9
4. Li YL, Zhang JX, Qiao GJ, Jin ZH (2005) Mater Sci Eng A 397:35. doi:10.1016/j.msea.2005.01.038
5. Wang XD, Qiao GJ, Jin ZH (2004) J Am Ceram Soc 87:565. doi:10.1111/j.1551-2916.2004.00565.x
6. Baskaran S, Halloran JW (1993) J Am Ceram Soc 76:2217. doi:10.1111/j.1151-2916.1993.tb07757.x
7. Padture NP, Evans CJ, Hockin HKX, Lawn BR (1995) J Am Ceram Soc 78:215. doi:10.1111/j.1151-2916.1995.tb08386.x
8. Davis JB, Marshall DB, Housley RM, Morgan PED (1998) J Am Ceram Soc 81:2169. doi:10.1111/j.1151-2916.1998.tb02602.x
9. Suganuma K, Sasaki G, Fujita T, Okumura M, Niihara K (1993) J Mater Sci 28:1175. doi:10.1007/BF01191949
10. Kawai C, Yamakawa A (1997) J Am Ceram Soc 80:2705. doi:10.1111/j.1151-2916.1997.tb03179.x
11. Barsoum MW, El-Raghy T (1996) J Am Ceram Soc 79:1953. doi:10.1111/j.1151-2916.1996.tb08018.x
12. Shi ZQ, Wang JP, Qiao GJ, Jin ZH (2008) Mater Sci Eng A 492:29. doi:10.1016/j.msea.2008.03.004
13. Lawn BR, Padture NP, Cai HD, Guiberteau F (1994) Science 263:1114. doi:10.1126/science.263.5150.1114
14. Kusunose T, Sekino T, Choa YH, Niihara K (2002) J Am Ceram Soc 85:2689. doi:10.1111/j.1151-2916.2002.tb00515.x
15. Cai HD, Kalceff MAS, Lawn BR (1994) J Mater Res 9:762. doi:10.1557/JMR.1994.0762
16. Xu HHK, Jahanmir S (1995) J Am Ceram Soc 78:497. doi:10.1111/j.1151-2916.1995.tb08831.x

17. Padture NP (1994) J Am Ceram Soc 77:519. doi:10.1111/j.1151-2916.1994.tb07024.x
18. Fischer-Cripps AC, Lawn BR (1996) J Am Ceram Soc 79:2609. doi:10.1111/j.1151-2916.1996.tb09023.x
19. Latella BA, O'Connor BH, Padture NP, Lawn BR (1997) J Am Ceram Soc 80:1027. doi:10.1111/j.1151-2916.1997.tb02940.x
20. Lawn BR (1998) J Am Ceram Soc 81:1977. doi:10.1111/j.1151-2916.1998.tb02580.x
21. Zhang ZF, He G, Eckert J, Schultz L (2003) Phys Rev Lett 91:045505. doi:10.1103/PhysRevLett.91.045505
22. Yoon YS, Na SW, Lee J, Cho MW, Lee ES, Cho WS (2004) J Am Ceram Soc 87:1374. doi:10.1111/j.1151-2916.2004.tb07740.x
23. Cho WS, Cho MW, Lee JH, Munir ZA (2006) Mater Sci Eng A 418:61. doi:10.1016/j.msea.2005.11.033
24. Jiang T, Jin ZH, Yang JF, Qiao GJ (2008) Mater Sci Eng A 494:203. doi:10.1016/j.msea.2008.04.047